Magnetic ordering and structural distortion in a PrFeAsO single crystal studied by neutron and x-ray scattering

M. G. Kim, W. Ratcliff, II, D. M. Pajerowski, J.-W. Kim, J.-Q. Yan, J. W. Lynn, A. I. Goldman, and A. Kreyssig

Phys. Rev. B **103**, 174405 — Published 5 May 2021

DOI: 10.1103/PhysRevB.103.174405

Magnetic ordering and structural distortion in PrFeAsO single crystal studied by neutron and x-ray scattering

M. G. Kim,[1,2,3,*] W. Ratcliff II,[4] D. M. Pajerowski,[4] J.-W. Kim,[5] J.-Q. Yan,[3,†] J. W. Lynn,[4] A. I. Goldman,[3] and A. Kreyssig[3]

[1]*Department of Physics, University of Wisconsin-Milwaukee, Milwaukee, WI 53201, USA*
[2]*Department of Physics and Astronomy, Rutgers University, Piscataway, New Jersey 08854, USA*
[3]*Ames Laboratory, U.S. DOE and Department of Physics and Astronomy, Iowa State University, Ames, IA 50011, USA*
[4]*NIST Center for Neutron Research, National Institute of Standards and Technology, Gaithersburg, Maryland 20899, USA*
[5]*Advanced Photon Source, Argonne National Laboratory, Argonne, Illinois 60439, USA*

(Dated: April 19, 2021)

We report the magnetic ordering and structural distortion in PrFeAsO crystals, the basis compound for one of the oxypnictide superconductors, using high-resolution x-ray diffraction, neutron diffraction, and x-ray resonant magnetic scattering (XRMS). We found the structural tetragonal-to-orthorhombic phase transition at $T_{\rm S}$ = 147 K, the AFM phase transition of the Fe moments at $T_{\rm Fe}$ = 72 K, and the Pr AFM phase transition at $T_{\rm Pr}$ = 21 K. Combined high-resolution neutron diffraction and XRMS show unambiguously that the Pr moments point parallel to the longer orthorhombic ***a*** axis and order antiferromagnetically along the ***a*** axis but ferromagnetically along the ***b*** and ***c*** directions in the stripe-like AFM order. The temperature dependent magnetic order parameter of the Pr moments shows no evidence for a reorientation of moments.

I. INTRODUCTION

Magnetism is generally considered detrimental to superconductivity because the magnetic fields produced by spins can break the Bosonic bond (the so-called Cooper pair) or polarize electrons' spin, which disturbs pairing between electrons. On the contrary, in the Fe-based (pnictide) superconductors, it is argued that the Cooper pairing mechanism is mediated by the antiferromagnetic (AFM) spin fluctuations originated from the Fe magnetism while the AFM competes with SC for the same electrons in the system.[1–4] Subtle balance in the correlation is a key for the unconventional superconductivity in pnictide superconductors.

Among the various families of the pnictide superconductors, the oxypnictide compounds (e.g. *RE*FeAsO with *RE* = Rare-Earth) are in a unique position due to the rare-earth magnetism. The first discovered oxypnictide superconductor is composed of the non-magnetic La element ($LaFeAsO_{1-x}F_x$) which shows a relatively high superconducting transition temperature ($T_{\rm c}$) at $\sim$ 26 K.[5] As several magnetic rare-earth elements can form the oxypnictide compounds, $T_{\rm c}$ is raised to $\sim$ 41 K for Ce,[6] $\sim$ 44 K for Pr,[7] $\sim$ 49 K for Nd[8] and $\sim$ 55 K for Sm[9] in REFeAs$O_{1-x}F_x$. Such increases in $T_{\rm c}$ may be related with geometric factors due to the Lanthanide contraction.[2,10,11] Another possibility is the rare-earth magnetism which influences the AFM spin fluctuations of Fe through an interplay between the rare-earth and the Fe magnetism[1–4,12–23] and results in the enhancement of $T_{\rm c}$.

Reviews on the variation in the geometric factors show a correlation between $T_{\rm c}$ and the As-Fe-As bond angle; $T_{\rm c}$ seems to be the highest within each family of compounds when the bond angle is set close to the ideal angle, 109.5°.[2,10,11] Intriguingly, among various materials which are found to have the bond angle very close to the ideal angle, the higher superconducting transition temperatures occur in the rare-earth oxypnictide compounds. This implies the potential importance of the rare-earth magnetism in the unconventional superconductivity in the family of *RE*FeAsO compounds. Therefore, it is essential to know the precise magnetic structures of the rare-earth oxypnictides.

Here, we report the magnetic ordering and structural distortion in one of the parent compounds of the oxypnictide superconductors, PrFeAsO. Earlier studies on PrFeAsO showed a structural transition from the tetragonal *P4/mmm* to the orthorhombic *Cmme* below $T_{\rm S} \approx$ 150 K.[13–15] The stripe antiferromagnetic ordering of Fe at $T_{\rm Fe} < T_{\rm S}$ followed by the Pr magnetic ordering below $T_{\rm Pr} \approx$ 15 K were also reported.[13–15] Neutron powder diffraction (NPD) measurements reported that the Pr moment points along the ***c*** axis with ferromagnetically coupled moments in the ***ac*** plane which are antiferromagnetically aligned along the ***b*** direction[13,14] but a μSR study claimed a similar magnetic arrangement along each crystallographic axis except the Pr moments pointing along the ***a*** axis.[15] Our study using high-resolution x-ray diffraction, neutron diffraction, and x-ray resonant magnetic scattering (XRMS) reveals that the structural transition, the Fe AFM order, and the Pr AFM order are consistent with the previous reports. However, combined high-resolution neutron diffraction and XRMS show unambiguously that the Pr moments are pointing parallel to the longer orthorhombic ***a*** axis and order antiferromagnetically along the ***a*** axis but ferromagnetically along the ***b*** and ***c*** directions. The temperature dependent magnetic order parameter of the Pr moments shows no evidence of a moment reorientation which was observed in the SmFeAsO and NdFeAsO compounds.[22,24]

II. EXPERIMENT

Single crystals of PrFeAsO were grown out of a NaAs flux using the conventional high temperature solution growth technique as described in Ref. 25. The stoichiometry of samples from a growth batch was examined by wavelength dispersive spectroscopy in a JEOL JXA-8200 Superprobe electron probe microanalyzer. Temperature-dependent, high-resolution x-ray diffraction measurements were performed on a four-circle diffractometer using Cu $K\alpha_1$ radiation from a rotating-anode

x-ray source, selected by a germanium (1, 1, 1) monochromator. An as-grown plate-like single crystal with dimensions of approximately 2 × 2 × 0.08 mm^3 of mass m = 4.6 mg was attached to a flat copper sample holder on the cold finger of a closed-cycle helium refrigerator. The sample was aligned such that the low-temperature orthorhombic (H, 0, L) reciprocal lattice planes were coincident with the scattering plane. In this paper, we will generally use the orthorhombic notation (H, 0, L) and, where necessary, employ the tetragonal notation (h, h, l)$_{\rm T}$ with a subscript "T". The diffraction data were obtained as a function of temperature between 160 K and 5 K, the base temperature of the refrigerator.

Single-crystal neutron diffraction measurements were carried out using the BT7[26] and BT9 thermal-neutron triple-axis spectrometer at NCNR, NIST. The same m = 4.6 mg single crystal was mounted on a thin aluminum plate, oriented in the orthorhombic (H, 0, L) plane, and placed in a liquid helium dilution refrigerator. The beam collimators before the monochromator, between the monochromator and sample, between the sample and analyzer, and between the analyzer and detector were 40′– 48′– 40′– open, respectively. A fixed incident neutron energy of 14.7 meV (λ = 2.359 Å) was used, and two pyrolytic graphite (PG) filters were employed to effectively eliminate higher harmonics in the incident beam. For high-resolution measurements, a collimation of 10′– 10′– 10′– 40′ was used. All measurements were performed between 130 K and 2 K, the base temperature of the refrigerator.

The XRMS experiment was conducted on the beam line 6-ID-B at the Advanced Photon Source at Argonne National Laboratory at the Pr L_2 edge (E = 6.44 keV). The incident radiation was linearly polarized perpendicular to the vertical scattering plane (σ polarized) with a spatial cross section of 0.5 mm (horizontal) × 0.2 mm (vertical) defined by a set of slits before the sample. In this configuration, dipole resonant magnetic scattering rotates the scattered beam polarization into the scattering plane (π polarization). Cu(2, 2, 0) was used as a polarization and energy analyzer to suppress the charge and fluorescence background relative to the magnetic scattering signal. The same sample (2 × 2 × 0.08 mm^3, m = 4.6 mg) was initially mounted at the end of the cold finger of a closed cycle Joule-Thomson cryostat (3 K ≤ T ≤ 18 K) with the orthorhombic (H, 0, L) or (0, K, L) planes coincident with the scattering plane and the [0, 0, L] direction as specular direction.

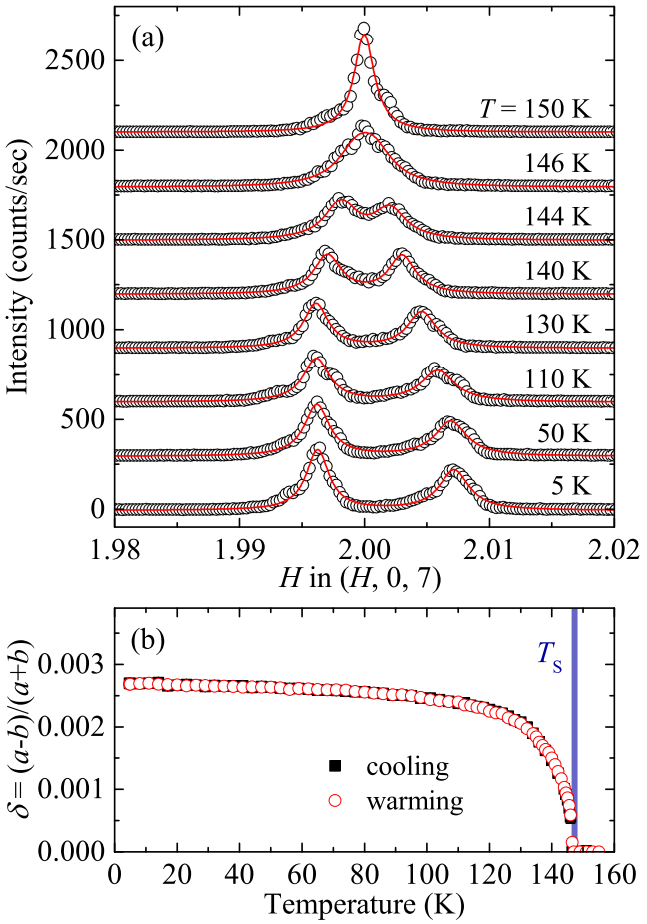

FIG. 1. (a) High-resolution x-ray diffraction scans along the [H, 0, 0] direction through (2, 0, 7) charge Bragg peak for selected temperatures. The lines present the fitted curves using Lorentzian-squared line shapes. (b) Orthorhombic distortion, determined from fits to the (2, 0, 7) and (0, 2, 7)′ charge Bragg peaks, as a function of temperature upon cooling and warming. The blue bar indicates the tetragonal-to-orthorhombic structural transition temperature ($T_{\rm S}$). Error bars are smaller than symbols and represent one standard deviation.

III. RESULTS

In Fig. 1 (a), we display representative [H, 0, 0] scans through the (2, 0, 7) charge Bragg peak position between 150 K and 5 K, obtained using the laboratory x-ray source, for PrFeAsO compound. Above the structural transition temperature $T_{\rm S}$ = 147 ± 1 K, we observe a sharp, single peak which is consistent with the tetragonal phase. Upon cooling below $T_{\rm S}$, the (2, 0, 7) charge Bragg peak continuously broadens and, then clearly splits into two peaks below T = 144 K, which are consistent with the orthorhombic phase. The splitting of the two orthorhombic charge Bragg peaks evolves rapidly with further cooling down to $T \approx$ 130 K. Then, the two peaks split apart gradually as temperature decreases. We fit the (2, 0, 7) and (0, 2, 7)′ Bragg peaks using the Lorentzian-squared line shape and summarize the result using the orthorhombic distortion $\delta = (a\text{-}b)/(a\text{+}b)$ in Fig. 1 (b). The orthorhombic distortion during cooling and warming does not show any hysteresis. We find a continuous transformation within the sensitivity of our measurements, which evidences the second order nature of the structural phase transition.

We now turn to the magnetic ordering of the PrFeAsO compound. Figure 2 (a) shows the temperature evolution of the (1, 0, 1) magnetic neutron diffraction peak at selected temperatures, and the magnetic order parameter measured at the same Bragg peak is shown as a function of temperature in Fig. 2 (b). We find that the (1, 0, 1) magnetic Bragg peak appears below $T_{\rm Fe} \approx$ 72 K and grows rapidly as tempera-

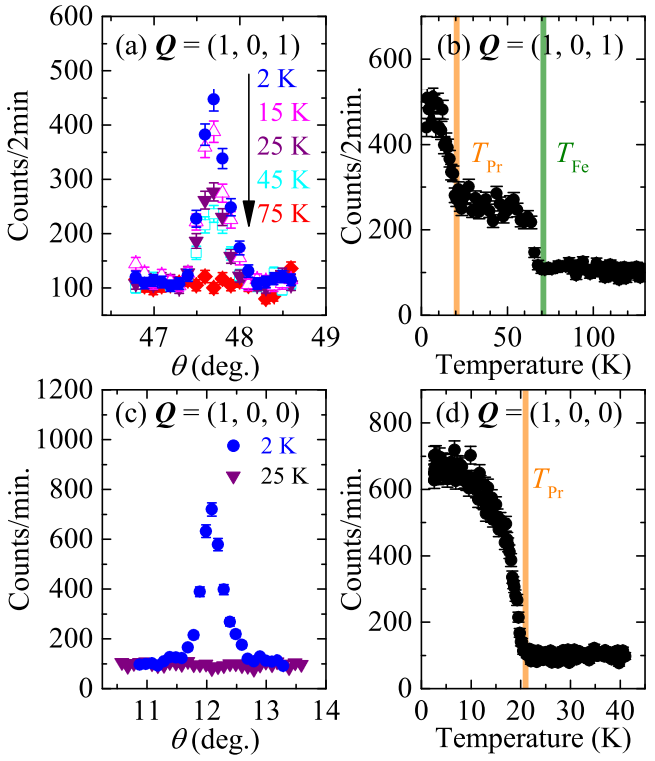

FIG. 2. Neutron diffraction rocking scans through (a) the (1, 0, 1) magnetic Bragg peak and (c) the (1, 0, 0) magnetic Bragg peak measured at selected temperatures. Temperature evolution of magnetic Bragg peak intensity measured (b) at (1, 0, 1) magnetic Bragg peak and (d) at (1, 0, 0) magnetic Bragg peak. Fe ordering temperature ($T_{\rm Fe}$) and Pr ordering temperature ($T_{\rm Pr}$) are marked with a green bar and orange bars, respectively.

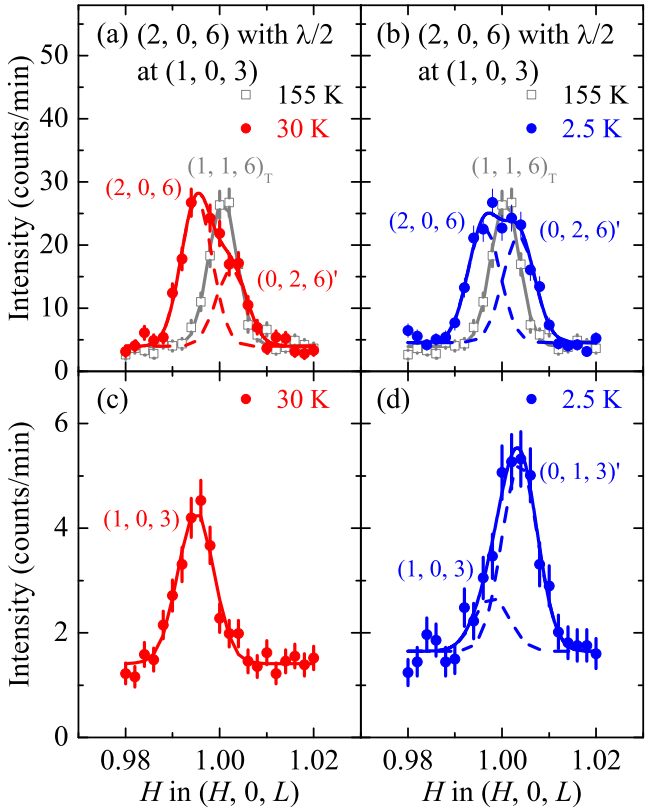

FIG. 3. High-resolution neutron diffraction scans along [H, 0, 0] through (a, b) the (2, 0, 6) nuclear Bragg peak measured with the second-harmonic of the incident neutrons ($\frac{\lambda}{2}$) and (c, d) the (1, 0, 3) and (0, 1, 3)$'$ magnetic Bragg peaks measured with the primary neutrons (λ). Open symbols are data measured at T = 155 K. Filled circles are data taken at T = 30 K in (a, b) and T = 2.5 K in (c, d). The magnetic peaks are fitted with one or two Gaussian line shapes. Resulting fits are shown with solid lines. Dashed lines present two-Gaussian fits.

ture decreases down to $\sim$ 60 K. Then the intensity increases monotonously until it raises abruptly again below $T_{\rm Pr} \approx$ 21 K. This observation is consistent with the AFM propagation vector $\boldsymbol{Q}_{\rm Fe,AFM}$ = (1, 0, 1) for the Fe order reported in literature.[13–15] We find another magnetic Bragg peak at $\boldsymbol{Q}$ = (1, 0, 0) below $T \approx$ 21 K [Fig. 2 (c)]. Its temperature dependence shows a typical behavior for an AFM order parameter [Fig. 2 (d)], and it is consistent with previously reported Pr magnetic order with $\boldsymbol{Q}_{\rm Pr,AFM}$ = (1, 0, 0). We conclude that the Fe order appears at $\boldsymbol{Q}_{\rm Fe,AFM}$ = (1, 0, 1) below $T_{\rm Fe} = 72 \pm 1$ K followed by the Pr order at $\boldsymbol{Q}_{\rm Pr,AFM}$ = (1, 0, 0) below $T_{\rm Pr} = 21 \pm 1$ K.

The Fe order appears at a low temperature ($T_{\rm Fe} = 72 \pm 1$ K) compared to the much higher structural transition temperature, $T_{\rm S}$ = 147 K. Such a large difference between $T_{\rm Fe}$ ($\equiv T_{\rm N}$) and $T_{\rm S}$ is unusual; the temperature difference is typically within several degrees in most of the undoped, parent pnictide compounds. A similar low $T_{\rm Fe}$ was previously reported by a NPD measurement[13] while other studies showed higher $T_{\rm Fe}$ which is closer to $T_{\rm S}$.[14] The discrepancy in $T_{\rm Fe}$ may be attributed to a sample-to-sample variation caused by different sample preparation processes. The phase diagrams of fluorine doped or oxygen deficient PrFeAsO compounds show that $T_{\rm S}$ decreases slowly while the reduction in $T_{\rm Fe}$ is rapid with increasing the level of F doping or oxygen deficiency.[27,28] Our sample indeed shows a slightly lower $T_{\rm S}$ than previously reported values for the undoped PrFeAsO. It implies a possible oxygen deficiency or unidentified dopant inclusion in our sample. This can explain our observation of much reduced $T_{\rm Fe} = 72$ K. Nonetheless, $T_{\rm Pr} = 21 \pm 1$ K from our neutron diffraction is consistent with previous reports.[13,14]

To further elucidate the magnetic ordering in PrFeAsO, we performed high-resolution neutron diffraction measurements which enable us to correctly identify positions of nuclear ($\equiv$ chemical structure) and magnetic Bragg peaks. We used the primary neutrons (λ) for magnetic Bragg peak and the second-harmonic neutrons ($\frac{\lambda}{2}$) by removing one PG filter for nuclear Bragg peak measurements. Above $T_{\rm S}$, a sharp, resolution-limited, single $(1, 1, 6)_T$ nuclear Bragg peak is observed at T = 155 K [Figs. 3 (a) and (b)]. As temperature decreases below $T_{\rm S}$, the tetragonal-to-orthorhombic distortion splits the $(1, 1, 6)_{\rm T}$ Bragg peak into two orthorhombic Bragg peaks, (2, 0, 6) and (0, 2, 6)$'$ related to the two domain orientations

with the longer orthorhombic ***a*** axis and shorter orthorhombic ***b*** axis. Generally, neutron diffraction measurements do not provide a sufficient spatial resolution to resolve the two orthorhombic peaks in this compound due to the small distortion. However, our high-resolution neutron diffraction provides a spatial resolution that is sufficient to discern two peaks from the measurements. At T = 30 K and 2.5 K in Figs. 3 (a) and (b), we observed broad signals that are almost two times broader than the resolution-limited $(1, 1, 6)_{\rm T}$ Bragg peak at T = 155 K. The signals cannot be described by any single line-shape commonly used in diffraction experiments and apparently are described well with two Gaussian lineshapes for (2, 0, 6) and $(0, 2, 6)'$. We note slightly different peak shapes between the data at T = 30 K and 2.5 K. The difference is because the (2, 0, 6) and $(0, 2, 6)'$ nuclear Bragg peaks were measured at the $\boldsymbol{Q}$ = (1, 0, 3) Bragg peak position with the PG filters removed to use the second-harmonic neutrons ($\frac{\lambda}{2}$) where the (1, 0, 3) and/or $(0, 1, 3)'$ magnetic Bragg peak intensities (described below) from the primary neutrons (λ) contribute to the intensities in the nuclear Bragg peak $\boldsymbol{Q}$ scans.

Figures 3 (c) and (d) show the magnetic Bragg peaks at T = 30 K and 2.5 K, respectively. At 30 K, the magnetic intensity appears around the $\boldsymbol{Q}$ position corresponding to the $(2, 0, 6)_{\lambda/2}$ nuclear Bragg peak; it is the (1, 0, 3) magnetic Bragg peak [Fig. 3 (c)]. Interestingly, at T = 2.5 K a magnetic peak appears around the position corresponding to the $(0, 2, 6)'_{\lambda/2}$ nuclear Bragg peak, compare peak positions between Fig. 3 (b) and (d). We also find that this peak is slightly broader than the peak measured at 30 K and successfully fitted with two Gaussian line-shapes, which indicate an existence of another magnetic Bragg peak at the position corresponding to the $(2, 0, 6)_{\lambda/2}$ nuclear Bragg peak. In other words, the observed magnetic signals at T = 2.5 K consist of (1, 0, 3) (with the smaller intensity) and $(0, 1, 3)'$ (with the larger intensity) magnetic Bragg peaks. This is a new observation that has not been observed in other neutron scattering experiments in this family of compounds.

The sharp, resolution-limited (1, 0, 3) magnetic Bragg peak at 30 K is consistent with the stripe AFM structure of the Fe moments in PrFeAsO. The smaller (1, 0, 3) intensity at 2.5 K can be seen as a reduction of the (1, 0, 3) magnetic peak at 30 K. It is possibly due to either a decrease of the Fe ordered moment or a reorientation of Fe moments at lower temperature. Reported NPD measurements indicate no change in the ordered moment size of Fe at low temperature.[13,14] We attempted searching for magnetic Bragg peak intensities in the $(H, 0, L)$ scattering plane that might be originated from the reorientation of Fe moments at T = 2.5 K but did not find any evidence of a reorientation of the Fe moments. Further investigation is required to construct the Fe moment configuration at low temperature. The known Pr ordering vector, $\boldsymbol{Q}_{\rm Pr,AFM}$ = (1, 0, 0), alone is sufficient to explain the appearance of the (1, 0, 3) and $(0, 1, 3)'$ magnetic Bragg peaks at T = 2.5 K. However, since different Pr moment configurations can produce magnetic intensities at $(H, 0, L)$ and $(0, K, L)'$ simultaneously, this set of measurements can not solve the exact Pr magnetic structure. In addition, because neutrons probe all moments, both Fe and Pr in the system, identifying a magnetic structure of Pr moments separately is extremely difficult using a small number of neutron scattering data.

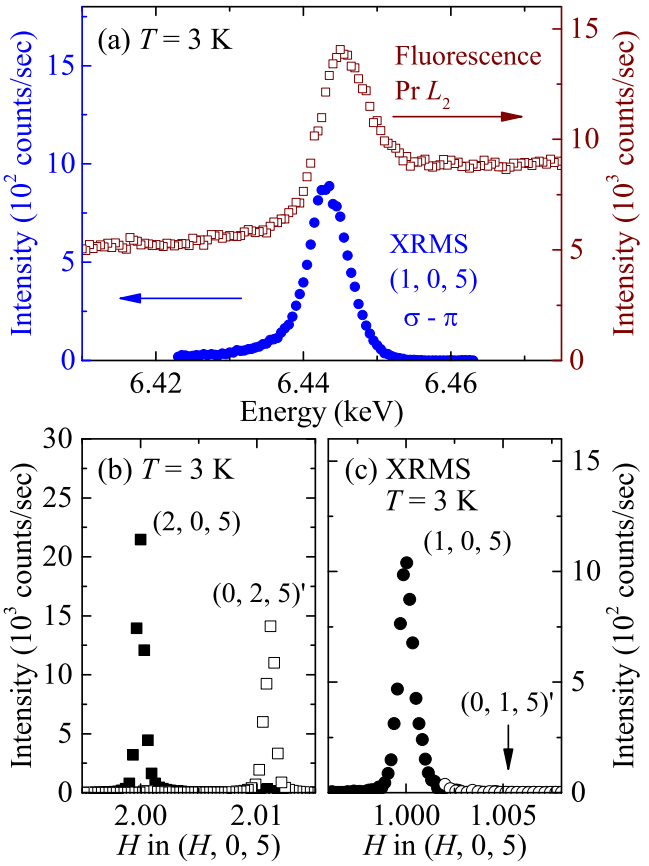

FIG. 4. (a) Energy scans through the (1, 0, 5) magnetic peak (filled circles) in the $\sigma - \pi$ scattering geometry at T = 3 K and the measured fluorescence (open squares) under the same experimental conditions without a polarization analyzer. (b) Distribution of structural Bragg peaks at T = 3 K measured along $[H, 0, 0]$ after the alignment is optimized for $\boldsymbol{Q}$ = (2, 0, 5) (filled squares) and $(0, 2, 5)'$ Bragg peaks (open squares). (c) Magnetic Bragg peaks at T = 3 K measured along $[H, 0, 0]$ at positions corresponding to the (2, 0, 5) and $(0, 2, 5)'$ Bragg peaks. A magnetic Bragg peak appears only at $\boldsymbol{Q}$ = (1, 0, 5) (filled circles) but not at $\boldsymbol{Q}$ = $(0, 1, 5)'$ (open circles).

For a determination of the Pr magnetic structure, we employed the element-specific x-ray resonant magnetic scattering (XRMS) technique that can probe Pr magnetism separately from Fe magnetism by tunning the incoming x-ray energy to the Pr L_2 absorption edge. Figure 4 (a) displays the resonant behavior measured at T = 3 K and at the (1, 0, 5) magnetic Bragg peak position together with the fluorescence signal obtained under the same experimental conditions. In the energy spectrum, we observed an enhanced intensity in the $\sigma - \pi$ scattering channel which indicates the dipole ($E1$) resonance. It may also contain a contribution from quadruple ($E2$) allowed transitions. A clear separation of the $E1$ and $E2$ contributions will require further measurements in the $\sigma - \sigma$ channel.

The charge ($\equiv$ nuclear) Bragg peaks were measured at T

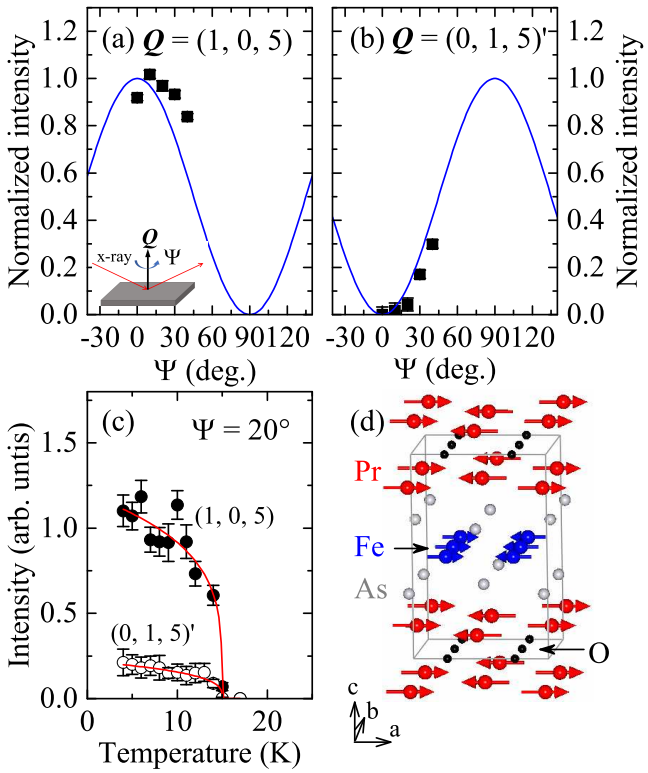

FIG. 5. Azimuthal angle ($0^\circ \leq \Psi \leq 40^\circ$) dependence of the normalized magnetic Bragg peak intensity measured at (a) $\boldsymbol{Q}$ = (1, 0, 5) and (b) (0, 1, 5)$'$ at T = 3K. Inset shows the schematic diagram of our experimental setup for the azimuthal angle scans. Lines present calculations using the Sine-squared function. (c) Temperature dependent XRMS signals at $\boldsymbol{Q}$ = (1, 0, 5) (filled symbols) and (0, 1, 5)$'$ (open symbols) with $\Psi = 20^\circ$. The lines present guides to the eye. (d) Proposed magnetic structure at T = 3 K with Pr moments pointing along the longer orthorhombic $\boldsymbol{a}$ axis.

= 3 K for (2, 0, 5) and (0, 2, 5)$'$ in Fig. 4 (b). Several angle scans were performed to optimize the intensity of each charge peak to estimate precise domain population of the orthorhombic twin domains. The intensity ratio between the (2, 0, 5) and (0, 2, 5)$'$ peaks is 1:0.84, indicating an approximately 1.2 times larger domain population related to the (2, 0, 5) Bragg peak than for the (0, 2, 5)$'$ Bragg peak. Then we searched magnetic reflections around the (1, 0, 5) and (0, 1, 5)$'$ Bragg positions at 3 K and find magnetic intensities only at the (1, 0, 5) Bragg peak position and not around the (0, 1, 5)$'$ Bragg peak position, see Fig. 4 (c). In the $\sigma - \pi$ scattering channel, the magnetic scattering intensity is sensitive to moments lying in the scattering plane and produces zero intensity for moments pointing out of the scattering plane. The absence of magnetic reflection around the (0, 1, 5)$'$ Bragg peak position, thus, indicates that the Pr moment is aligned perpendicular to $\boldsymbol{Q}$ = (0, 1, 5)$'$. Therefore, the Pr moments point along the orthorhombic $\boldsymbol{a}$ axis.

We obtained the azimuthal angle dependence of the scattered intensities at $\boldsymbol{Q}$ = (1, 0, 5) and (0, 1, 5)$'$ magnetic Bragg peak positions to identify the precise Pr moment direction. The azimuthal dependence was measured by rotating the sample about the scattering vector $\boldsymbol{Q}$ by an angle Ψ (consequently, the scattering plane varies) as shown in the inset in Fig. 5 (a). By the azimuthal rotation, moments are rotated with respect to the fixed scattering plane which changes the amplitude of the moment component projected in the scattering plane. We show intensities of the (1, 0, 5) and (0, 1, 5)$'$ magnetic Bragg peaks as a function of a limited range of azimuthal angles, $0^\circ \leq \Psi \leq 40^\circ$, in Fig. 5 (a) and (b). The solid black symbols are the measured azimuthal dependence and the blue lines are the sine-squared function for a collinear Pr moment arrangement along the orthorhombic $\boldsymbol{a}$ axis. We find that the azimuthal dependence of the (1, 0, 5) and (0, 1, 5)$'$ magnetic Bragg peaks is consistent with the Pr moment confined in the $\boldsymbol{ab}$ plane and pointing along the longer orthorhombic $\boldsymbol{a}$ axis as shown in Fig. 5 (d). Despite the small deviation of the measured azimuthal dependence from the calculation, the absence of the magnetic Bragg intensity at (0, 1, 5)$'$ at $\Psi = 0^\circ$clearly indicates that the Pr moments are aligned along the longer orthorhombic $\boldsymbol{a}$ axis. Our Pr magnetic structure is different from previous magnetic structures proposed by NPD. The neutron magnetic intensities were calculated for the (1, 0, 3) and (0, 1, 3)$'$ magnetic peaks based on our Pr magnetic structure, which gives a ratio between (0, 1, 3)$'$ and (1, 0, 3) to be $I_{(0,1,3)'}/I_{(1,0,3)}$ = 3.3. We get $I_{(0,1,3)'}/I_{(1,0,3)}$ = 3.5(7) from the observed intensities in Fig. 3 (d), which is consistent with our Pr magnetic structure.

Temperature dependencies of the magnetic peaks were measured with the azimuthal angle $\Psi = 20^\circ$. $\Psi = 20^\circ$ allows contributions from both (1, 0, 5) and (0, 1, 5)$'$ magnetic Bragg peaks and the result is displayed in Fig. 5 (c). We find that the magnetic order parameter at both Bragg peaks shows a similar power law behavior, indicating no reorientation of Pr moments in this temperature range. The observed Pr ordering temperature is $T_{\rm Pr} = 15 \pm 1$ K, which is slightly smaller than $T_{\rm Pr}$ measured by neutrons on the same sample. We believe that this is due to the x-ray beam heating effect.

IV. CONCLUSION

In summary, we have studied the magnetic ordering and structural distortion in PrFeAsO using x-ray and neutron scattering measurements. Our high-resolution x-ray diffraction measurements found a continuous, second order structural transition from the high-temperature tetragonal to the low-temperature orthorhombic structure at $T_{\rm S} = 147 \pm 1$ K. We find that the Fe AFM order appears at $T_{\rm Fe} = 72 \pm 1$ K at $\boldsymbol{Q}_{\rm Fe,AFM}$ = (1, 0, 1) followed by the Pr order at $T_{\rm Pr} = 21 \pm 1$ K at $\boldsymbol{Q}_{\rm Pr,AFM}$ = (1, 0, 0). Together with the high-resolution neutron diffraction and the XRMS, we find that the Pr has a collinear antiferromangetic structure with moments pointing along the longer orthorhombic $\boldsymbol{a}$ axis. Our temperature dependent measurements on magnetic Bragg peaks from the Pr order show that the Pr magnetic structure remains the same in all the temperature range below $T_{\rm Pr}$.

Now we comment on the connection between the rare-earth magnetism and the superconductivity in the family of

*RE*FeAsO with *RE* = Ce, Pr, Nd, and Sm. In the case of the lighter rare-earth elements (Ce and Pr), their moments order in-plane; Ce in the CeFeAsO compound orders in a non-collinear AFM structure with moments lying in the ***ab*** plane[12,15] and Pr moments in PrFeAsO, pointing along the ***a*** direction, and form a collinear AFM structure. Similar in-plane moment arrangements of the rare-earth moment and the Fe moment may indicate a strong influence of the Fe moment on the rare-earth (Ce and Pr) moment. On the other hand, in heavier rare-earth elements (Nd and Sm), the moments of Nd and Sm order collinearly with their moments aligned in the ***c*** direction at low temperature. The interaction between the rare-earth and Fe moments yields not only a reorientation of the rare-earth moments but also of the Fe moments.[22,24] Interestingly, the superconducting transition temperatures are higher in the heavier rare-earth compounds. This implies that the rare-earth magnetism with their moment along the ***c*** direction and/or its strong influence on the Fe moment may be important for higher $T_{\rm c}$ in *RE*FeAsO. Higher $T_{\rm c}$ in $Gd_{1-x}Th_xFeAsO$ with the Gd moments along the ***c*** direction[29] is consistent with this scenario.

ACKNOWLEDGMENTS

Work at the Rutgers University was supported by the U.S. Department of Energy (DOE) under Grant No. DOE: DE-FG02-07ER46382. Work by the Ames group was supported by the Department of Energy, Basic Energy Sciences, Division of Materials Sciences and Engineering, under Contract No. DE-AC02-07CH11358. This research used resources of the Advanced Photon Source, a U.S. Department of Energy (DOE) Office of Science User Facility operated for the DOE Office of Science by Argonne National Laboratory under Contract No. DE-AC02-06CH11357. We acknowledge the support of the National Institute of Standards and Technology, U. S. Department of Commerce in providing facilities used in this work. The identification of any commercial product or trade name does not imply endorsement or recommendation by the National Institute of Standards and Technology.

* mgkim@uwm.edu
† Present Address: Materials Science and Technology Division, Oak Ridge National Laboratory, Oak Ridge, Tennessee 37831, USA

[1] J. W. Lynn and P. Dai, Physica C **469**, 469 (2009).
[2] D. C. Johnston, Adv. Phys. **59**, 803 (2010).
[3] M. D. Lumsden and A. D. Christianson, J. Phys.: Condens. Mat. **22**, 203203 (2010).
[4] P. Dai, Rev. Mod. Physics **87**, 855 (2015).
[5] H. M. Kamihara Y., Watanabe T. and H. H., J. Am. Chem. Soc. **130**, 3296 (2008).
[6] G. F. Chen, Z. Li, D. Wu, G. Li, W. Z. Hu, J. Dong, P. Zheng, J. L. Luo, and N. L. Wang, Phys. Rev. Lett. **100**, 247002 (2008).
[7] Z. A. Ren, J. Yang, W. Lu, W. Yi, G. C. Che, X. L. Dong, L. L. Sun, and Z. X. Zhao, Materials Research Innovations **12**, 105 (2008).
[8] Z.-A. Ren, J. Yang, W. Lu, Y. W., X.-L. Shen, Z.-C. Li, G.-C. Che, X.-L. Dong, L.-L. Sun, F. Zhou, et al., EPL **82**, 57002 (2008).
[9] Z.-A. Ren, W. Lu, J. Yang, Y. W., X.-L. Shen, Z.-C. Li, G.-C. Che, X.-L. Dong, L.-L. Sun, F. Zhou, et al., Chinese Phys. Lett. **25**, 2215 (2008).
[10] C.-H. Lee, A. Iyo, H. Eisaki, H. Kito, M. Teresa Fernandez-Diaz, T. Ito, K. Kihou, H. Matsuhata, M. Braden, and K. Yamada, J. Phys. Soc. Jpn. **77**, 083704 (2008).
[11] Y. Mizuguchi, Y. Hara, K. Deguchi, S. Tsuda, T. Yamaguchi, K. Takeda, H. Kotegawa, H. Tou, and Y. Takano, Supercond. Sci. Technol. **23**, 054013 (2010).
[12] J. Zhao, Q. Huang, C. de la Cruz, S. Li, J. W. Lynn, Y. Chen, M. A. Green, G. F. Chen, G. Li, Z. Li, et al., Nat. Mater. **7**, 953 (2008).
[13] S. A. J. Kimber, D. N. Argyriou, F. Yokaichiya, K. Habicht, S. Gerischer, T. Hansen, T. Chatterji, R. Klingeler, C. Hess, G. Behr, et al., Phys. Rev. B **78**, 140503 (2008).
[14] J. Zhao, Q. Huang, C. de la Cruz, J. W. Lynn, M. D. Lumsden, Z. A. Ren, J. Yang, X. Shen, X. Dong, Z. Zhao, et al., Phys. Rev. B **78**, 132504 (2008).
[15] H. Maeter, H. Luetkens, Y. G. Pashkevich, A. Kwadrin, R. Khasanov, A. Amato, A. A. Gusev, K. V. Lamonova, D. A. Chervinskii, R. Klingeler, et al., Phys. Rev. B **80**, 094524 (2009).
[16] Y. Chen, J. W. Lynn, J. Li, G. Li, G. F. Chen, J. L. Luo, N. L. Wang, P. Dai, C. dela Cruz, and H. A. Mook, Phys. Rev. B **78**, 064515 (2008).
[17] Y. Qiu, W. Bao, Q. Huang, T. Yildirim, J. M. Simmons, M. A. Green, J. W. Lynn, Y. C. Gasparovic, J. Li, T. Wu, et al., Phys. Rev. Lett. **101**, 257002 (2008).
[18] A. Marcinkova, E. Suard, A. N. Fitch, S. Margadonna, and J. W. G. Bos, Chem. Mater. **21**, 2967 (2009).
[19] M. A. McGuire, R. P. Hermann, A. S. Sefat, B. C. Sales, R. Jin, D. Mandrus, F. Grandjean, and G. J. Long, New J. Phys. **11**, 025011 (2009).
[20] D. H. Ryan, J. M. Cadogan, C. Ritter, F. Canepa, A. Palenzona, and M. Putti, Phys.l Rev. B **80**, 220503(R) (2009).
[21] W. Tian, W. Ratcliff, M. G. Kim, J.-Q. Yan, P. A. Kienzle, Q. Huang, B. Jensen, K. W. Dennis, R. W. McCallum, T. A. Lograsso, et al., Phys. Rev. B **82**, 060514 (2010).
[22] S. Nandi, Y. Su, Y. Xiao, S. Price, X. F. Wang, X. H. Chen, J. Herrero-Martín, C. Mazzoli, H. C. Walker, L. Paolasini, et al., Phys. Rev. B **84**, 054419 (2011).
[23] A. Marcinkova, T. C. Hansen, and J. W. G. Bos, J. Phys.: Condens. Mat. **24**, 256007 (2012).
[24] M. G. Kim, J.-W. Kim, J.-Q. Yan, A. I. Goldman, and A. Kreyssig, Phys. Rev. B **100**, 224401 (2019).
[25] J.-Q. Yan, S. Nandi, J. L. Zarestky, W. Tian, A. Kreyssig, B. Jensen, A. Kracher, K. W. Dennis, R. J. McQueeney, A. I. Goldman, et al., Appl. Phys. Lett. **95**, 222504 (2009).
[26] J. W. Lynn, Y. Chen, S. Chang, Y. Zhao, S. Chi, n. Ratcliff, W, B. G. Ueland, and R. W. Erwin, Journal of research of the National Institute of Standards and Technology **117**, 61 (2012).
[27] C. R. Rotundu, D. T. Keane, B. Freelon, S. D. Wilson, A. Kim, P. N. Valdivia, E. Bourret-Courchesne, and R. J. Birgeneau, Phys. Rev. B **80**, 144517 (2009).
[28] K. Kodama, M. Ishikado, F. Esaka, A. Iyo, H. Eisaki, and S.-i. Shamoto, J. Phys. Soc. Jpn. **80**, 034601 (2011).
[29] N. R. Lee-Hone, D. H. Ryan, J. M. Cadogan, Y. L. Sun, and G. H. Cao, J. Appl. Pjys. **115**, 17D705 (2014).